Development of a device useful to reproducibly produce large quantities of viable and uniform stem cell spheroids with controlled diameters

Biomaterials Advances 135 (2022) 112685

Contents lists available at ScienceDirect

Biomaterials Advances

journal homepage: www.elsevier.com/locate/bioadv

Development of a device useful to reproducibly produce large quantities of viable and uniform stem cell spheroids with controlled diameters

Monize Caiado Decarli [a,b], Mateus Vidigal de Castro [c], Júlia Adami Nogueira [d], Mariana Harue T. Nagahara [a], Cecília Buzatto Westin [a], Alexandre Leite R. de Oliveira [c], Jorge Vicente L. da Silva [d], Lorenzo Moroni [b], Carlos Mota [b], Ângela Maria Moraes [a,*]

[a] Department of Engineering of Materials and of Bioprocesses, School of Chemical Engineering, University of Campinas, Av. Albert Einstein, 500, 13083-852, Cidade Universitária "Zeferino Vaz", Campinas, SP, Brazil
[b] MERLN Institute for Technology-Inspired Regenerative Medicine, Department of Complex Tissue Regeneration, Maastricht University, Universiteitssingel, 40, Maastricht, the Netherlands
[c] Laboratory of Nerve Regeneration, University of Campinas, Cidade Universitária "Zeferino Vaz", Rua Monteiro Lobato, 255, 13083-862 Campinas, SP, Brazil
[d] Three-Dimensional Technologies Research Group, CTI Renato Archer, Rodovia Dom Pedro I SP-65, Km 143,6, 13069-901, Amarais, Campinas, SP, Brazil

ARTICLE INFO

Keywords:
3D cell culture
Cell spheroid
3D cell model
Stem cells
In vitro model
Microwell array
additive manufacturing

ABSTRACT

Three-dimensional cellular aggregates can mimic the natural microenvironment of tissues and organs and obtaining them through controlled and reproducible processes is mandatory for scaling up and implementing drug cytotoxicity and efficacy tests, as well as tissue engineering protocols. The purpose of this work was to develop and evaluate the performance of a device with two different geometries fabricated by additive manufacturing. The methodology was based on casting a microwell array insert using a non-adhesive hydrogel to obtain highly regular microcavities to standardize spheroid formation and morphology. Spheroids of dental pulp stem cells, bone marrow stromal cells and embryonic stem cells showing high cell viability and average diameters of around 253, 220, and 500 μm, respectively, were produced using the device with the geometry considered most adequate. The cell aggregates showed sphericity indexes above 0.9 and regular surfaces (solidity index higher than 0.96). Around 1000 spheroids could be produced in a standard six-well plate. Overall, these results show that this method facilitates obtaining a large number of uniform, viable spheroids with pre-specified average diameters and through a low-cost and reproducible process for a myriad of applications.

1. Introduction

Stem cell culture in two-dimensional environments has been extensively used and as such have become a standard procedure. It allows for the expansion of multi and pluripotent stem cells *in vitro* for different research and therapeutic purposes. However, 2D cell culture models are considered highly artificial since the native cell physiology and behavior can be significantly altered, not reflecting *in vivo* cell behavior [1–3]. Three-dimensional (3D) cellular aggregates can more effectively mimic the natural microenvironment of tissues and organs than 2D cell cultures, thus consisting of a feasible alternative for many purposes.

Drug efficacy tests [4–7] and cytotoxicity trials [8–11] have been currently performed using 3D models due to the differences in drug response between 2D and 3D cell models. The 3D cell culture systems present higher treatment resistance, more effectively reflecting the conditions of native tissues in comparison with conventional 2D monolayer models [2]. In addition, 3D models are also used to mimic different types of pathologies with great fidelity, consisting of a valuable tool to elucidate their mechanisms [12,13].

More recently, tissue engineering and biofabrication [14–16], and lately, bioprinting [17–19], have been applying *in vitro* 3D model aggregates as an alternative to cells in suspension. Frequently, stem cells spheroids are employed after a differentiation process to obtain the desired tissue, but spheroids obtained from primary progenitor cells of specific health tissues have also been used. Both 3D cell model approaches hold great potential for generating complex tissue-like constructs with advanced maturation state, capable of offering better regenerative properties, and their use has been increasing over the last twenty years [20,21]. As a result, several constructs have been produced using different spheroid-loaded bioprinting techniques, as recently reviewed by Mota et al. [18], such as cardiac patches, large single vessels, vessels with simple branching, nerve guides, salivary and thyroid glands, among others.

However, all those fields demand large quantities of 3D cell aggregates highly uniform in size and geometry, specifically when considering high-throughput applications [22–24], *in vivo* screening of compounds [25], engineering highly-complex tissue constructs [26], and use in preclinical trials [27,28].

* Corresponding author.
E-mail address: ammoraes@unicamp.br (Â.M. Moraes).

http://dx.doi.org/10.1016/j.msec.2022.112685
Received 6 August 2021; Received in revised form 20 December 2021; Accepted 22 January 2022
Available online 31 January 2022

To meet this demand, a set of spheroid characteristics should be strictly controlled [29]. The most relevant variables to control are cell aggregate dimensions and geometry. Based on molecular diffusional limitations, the larger the spheroid size, the greater the probability of occurrence of hypoxia and restriction of nutrient access by cells located in the innermost regions [30,31]. As the number cell layers increases in a spheroid, so do the metabolic gradients of oxygen, nutrients and metabolites. In severe conditions, cell necrosis can be detected in the core of the spheroid [32], followed by the release of toxic residues and proteases from apoptotic cells into the whole structure, severely reducing the overall spheroid viability. As a useful guideline, the effectiveness of mass transfer, and consequently, of cell viability, strongly depends on the spheroid size [30,33,34]. Moreover, substantial impact on the differentiation potential of stem cell spheroids, as well as their functions and the roles that regulate hMSC fate, can be affected by these metabolic gradients, as reviewed by Sart et al. [3].

Spheroids need to be highly uniform not only as an alternative to control with their nutritional and metabolic gradients, but also because heterogeneity in size represents an inherent source of variability regarding outcomes obtained in many application fields. In case of drug efficacy and cytotoxicity trials, for instance, large and small aggregates behave differently depending on the treatment applied. In spheroids of around 500 μm, a pathophysiological environment typical of solid tumors can be observed, what cannot be noticed in smaller spheroids, of around 300 μm [31,34]. In case of tissue engineering and biofabrication-related applications, spheroids may be used as building blocks to construct larger tissues [17]. Thus, it is essential that size is standardized before the implementation of a manufacturing technique to more properly reproduce the architecture of the desired tissue. When bioprinting is considered, the diameter of the nozzle is selected depending on the spheroid diameter [29]. Spheroids larger than the nozzle will not be extruded and often will clog the printer's outlet channel, disturbing the bioprinting process. In another situation, small spheroids can be easily lost through the meshes of fibrous scaffolds with large pores, which were designed to hold larger spheroids. Thus, high uniformity in size and geometry is an essential parameter to control.

Another set of properties to control for refers to spheroid surface characteristics, mostly regarding circularity, roughness, and homogeneity. The tendency of particle aggregates to form spherical structures minimizes surface area and free energy in the system [35,36]. In the case of cell aggregates, the formation of spherical structures is favored by spontaneous self-assembly due to interactions of cell-cell and cell-extracellular matrix interactions. However, the outcome of self-assembly can be greatly improved depending on the spheroid formation method used. Moreover, when the spheroid surface is affected, protuberances, appendices and satellite aggregates could develop on it or attach to it, preventing their successful application. This is particularly prejudicial in bioprinting processes, since two or more spheroids can attach to each other and also clog the printer's nozzle during bioink extrusion.

In the last years, conventional techniques have been used to obtain spheroids, most of them based on physical stimuli, such as gravity, surface tension and centrifugal force [37]. More recently, a few methods involving sophisticated tools and strategies have been used to develop devices that allow precise control of the properties mentioned above, such as through the use of bioreactors and microfluidic platforms [38–41]. Bioreactors, in particular, enable remarkable advantages in terms of scaling up; however, in them, the diameter dispersion of the spheroids can achieve high values, as their size is controlled by collisions between cells and stirring parameters [40]. Microfluidic platforms, on the other hand, enable precise control of shear stress and fluid elements [41], but scale-up is mostly dependent on the replication of unitary systems. Finding the ideal balance to obtain spheroids with controlled diameters in large quantities is a challenging task that may be possible by the integration of different techniques.

Here, we show the performance of an optimized device developed by our research group, which integrates additive manufacturing and molding techniques to create a reusable low-cost microwell array construct for culturing cells in a 3D microenvironment in a highly reproducible way. The array is produced through the use of a 3D printed rigid mold, which is employed to cast a biocompatible micromolded hydrogel array; this, in turn, is used as a microwell insert to form spheroids. To validate the versatility of this device in producing uniform and regular human cell spheroids, two different cell categories were chosen: adult human stem cells (from dental pulp and bone marrow) and human embryonic cells.

A few microwell array systems useful in the production of spheroids are already available in the market, such as ultra-low attachment plates, the Aggrewell system, and commercial hydrogel microwells. However, most of them are disposable systems and in all these cases the dimensions of the cavities are previously defined in a pre-fabricated array. With our device, we aim to provide a simple, reusable and customizable approach to offer the possibility of having a CAD design to modify the device accordingly to the need of the costumer, as well as to make available a low-cost methodology to obtain 3D cell models in large quantities for different *in vitro* study purposes. Thus, our system can be easily implemented and modified when necessary in the laboratory routine, consisting in a reliable *in vitro* alternative to minimize animal use. To this end, the main objective of this study was to evaluate the performance of an optimized device to standardize spheroid time frame formation with controlled geometry and high viability *in vitro*.

2. Methods

2.1. Mold device manufacture to obtain the microwell array insert

The methodology used consists of three main steps [42], as illustrated in Fig. 1. The first step (Fig. 1a) refers to the use of a computer-aided design (CAD) software, in which precise dimensions and geometry are defined by the user to create a multiple array of micropillars and a cup support. The 3D model is printed to serve as a rigid template (called herein as mold device) used to cast a biocompatible hydrogel construct (called microwell array insert), described in Fig. 1b. In the last step (Fig. 1c), the cells are seeded in the microwell array and after the aggregation and compaction phases, a high number of uniform spheroids can be obtained.

3D CAD modeling was performed with the Rhinoceros™ 3D 5.0 software (Robert McNeel and Associates, USA). Two independent parts were designed. The first part consisted of an array containing 164 micropillars; the second, of an open-bottom cup support with a sealing O-ring to prevent leakage and to facilitate demolding.

Each micropillar was designed to have a regular bottom-hexagon, with 570 μm side length and 1100 μm major diagonal followed by a top-hemisphere with 600 μm in diameter (Fig. 1d-e) so as to improve reproducible and homogeneous spheroid formation. Based on the same micropillar configuration, two different mold devices were designed, which are hereafter described as mold devices 1 and 2. Varying the array height (Fig. 1f), thickness (Fig. 1g), and cup support geometry (Fig. 1h), the mold device 2 was designed to offer higher volumetric capacity (Fig. 1i), so that three times more culture medium with cells in suspension could be used in comparison to mold device 1. The mold devices were manufactured using the rigid acrylate-based photopolymer Veroclear™ (Stratasys, Israel), by means of a Polyjet 3D printing technology (Objet Connex 350TM, Stratasys, Israel) and ultraviolet light for polymer curing.

Once manufactured, the mold device was mechanically cleaned with a high-pressure water jet and dried with compressed air. Device disinfection was performed in five steps, starting by washing with neutral 2% Extran™ MA (Merck Millipore, USA) detergent solution for 30 s, followed by washing with sterile distilled water, ethanol solution (70% *v*/v) for 5 min and finally, by rinsing with sterile distilled water. The excess water was removed with sterile paper wipes. Alternatively, the mold device may be sterilized by exposure to ethylene oxide.

2.2. Hydrogel formulations used to produce the microwell arrays by molding

Microwell arrays were manufactured from mold devices 1 and 2 as described above, and are hereafter termed microwell arrays 1 and 2, respectively. These microwell arrays were used as inserts of a regular 6-well cell

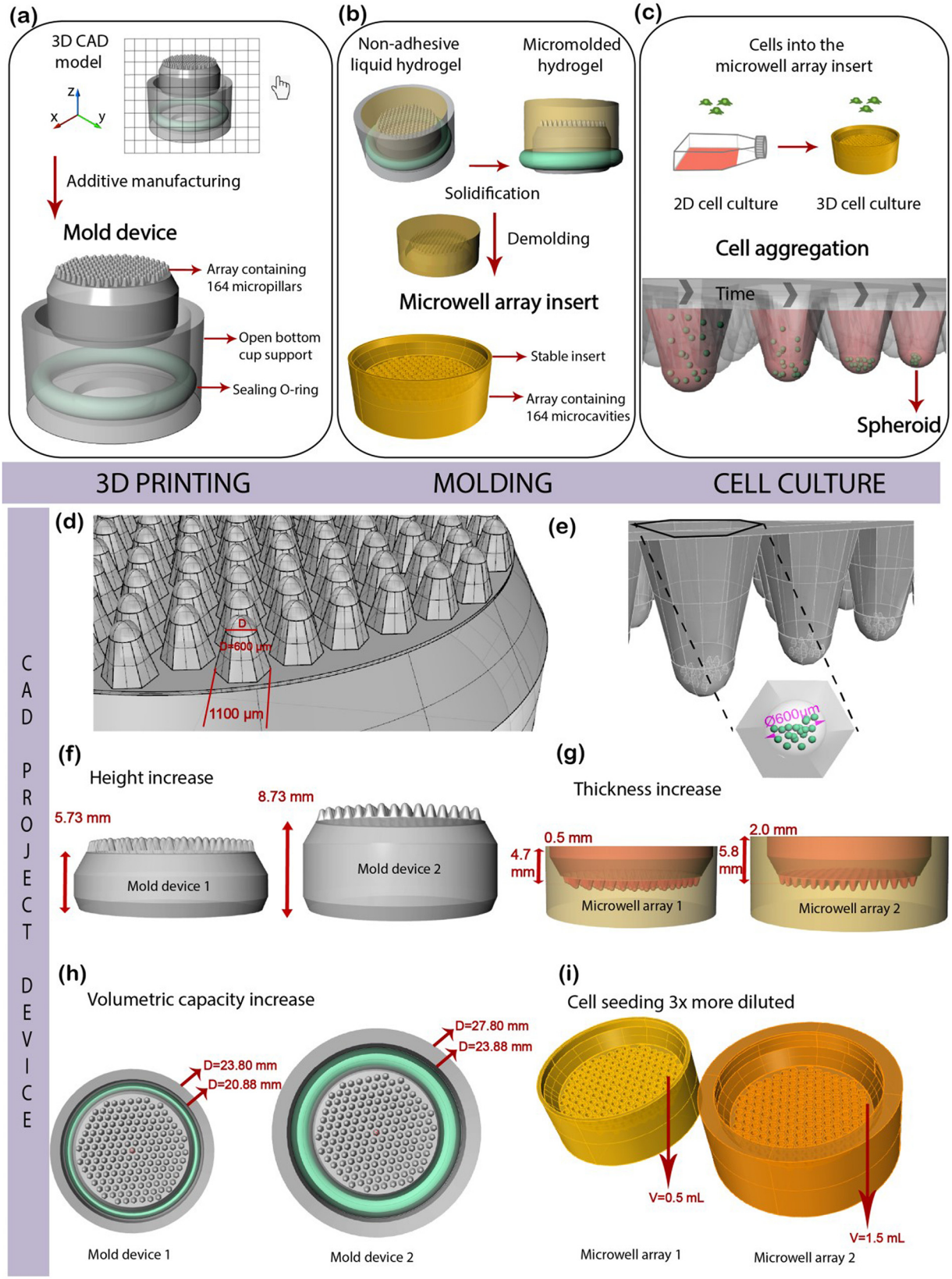

Fig. 1. Steps for the manufacture of mold devices 1 and 2 and the microwell array insert used to produce stem cell spheroids: a) schematic concept using computer-aided design and additive manufacturing approaches to produce the designed mold devices; b) solid microwell array insert is manufactured by casting a non-adhesive hydrogel; c) cell seeding and sedimentation lead to aggregation in spheroids; d-e) dimensional details of the micropillar array geometry, consisting of a hybrid shape made of a bottom hexagon pyramidal structure (1100 µm major diagonal, 570 µm side length) and a top defined by a semi-sphere (600 µm in diameter). Two CAD models were designed, in which different parameters were modified to improve mold device 1 and obtain mold device 2, in which: f) height was increased; g) thickness and stability of the peripheral rim were increased; h) O-ring size was increased; i) volume to perform cell seeding was increased three times, allowing cell suspension dilution.

culture plate and were produced using sterile ultrapure agarose (Sigma-Aldrich ref. A9539, lot# 071M0572V, USA) hydrogels, obtained by dissolving the polysaccharide in either 0.9% NaCl saline solution, PBS or αMEM supplemented with 10% fetal bovine serum (FBS) plus 1% penicillin/streptomycin (Pen-Strep) in different temperatures, as summarized in Table 1.

Since the Veroclear™ mold cannot be exposed to temperatures above 70 °C, 2 and 3% agarose in 0.9% (*w/v*) NaCl solutions were prepared at around 90 °C to ensure the complete dissolution of the polysaccharide and after being cooled to about 60 °C, the agarose solutions were poured into the mold device. Given that many FBS components can be significantly affected by heating up to 90 °C, this procedure could not be used to formulate agarose solutions in the supplemented culture medium. In this case, the samples were prepared by dissolving agarose in the culture medium through heating in a water bath at 56 °C, as this temperature is traditionally used in FBS heat-inactivation procedures, or at 37 °C, as used in standard stem cell culture protocols.

After selecting the processing temperature, the agarose concentration and the solvent to reach the aimed hydrogel mechanical stability, each prepared solution was poured into the mold devices at room temperature to acquire the desired shape. After 10 min, the flexible molded microwell array inserts were manually detached from the Veroclear™ mold, transferred to a 6-well plate and submerged in culture medium for equilibration. The microwell array inserts were kept in the incubator (37 °C, 5% CO_2) until further use.

After demolding, the mold devices were washed using distilled water, dried with paper tissues, and stored at room temperature. As the mold device is a reusable system, the 5-step device disinfection process described in Section 2.1 was repeated every time before manufacturing a new agar microwell array.

2.3. Analysis of the mechanical properties of the hydrogels and the stability of the microwell arrays

The mechanical properties of block specimens (cylinders with 1.6 cm diameter and 1.4 cm height) of the hydrogel formulations used to produce the microwell arrays were assessed by a non-confined compression test until 30% of deformation at 1 mm/s using a 5 N load cell (TX.XTPlus, Texture Technologies, USA) to determine the most adequate formulation regarding mechanical resistance and stability to handling.

To analyze the microwell array stability for long periods, the molded specimens were kept under supplemented culture medium in an incubator at 37 °C and 5% CO_2 for 2, 14 and 30 days. At each time point, 4 independent array inserts were inspected by optical microscopy and the dimensions of the hexagonal shaped microwells ($n = 10$) were measured using the Image J software (National Institutes of Health, USA). The regular hexagon diagonal, side and distance from side to side were determined and compared with those of inserts obtained immediately after demolding (day 0).

2.4. Cell populations tested and 2D culture conditions

Two adult and one embryonic human stem cell lines were used in this work to analyze the efficiency of the inserts to promote viable and uniform spheroid formation. Dental pulp stem cells (hDPSCs) from Lonza (PT-5025, lot 361,150) were kindly supplied by R-Crio Criogenia S. A. (Campinas, Brazil). Human mesenchymal stromal cells were obtained from the acetabulum of a donor (female, 69 years) who was undergoing total hip replacement surgery and gave informed consent for bone marrow biopsy, approved by the medical ethical testing commission (METC) of the Medical Spectrum Twente in Enschede, the Netherlands [43]. Human embryonic stem cells (hESCs) were obtained from the Masaryk University cell bank, Czech Republic.

For all experiments, the stem cells were cultured in T-flasks and kept at 37 °C under a 5% CO_2 atmosphere in different culture media, until reaching 70% confluence. hDPSCs were cultured with minimum essential medium Eagle (α-MEM, Gibco) supplemented with 10% (*v*/v) FBS (ref. F0804, Sigma-Aldrich), 1% (v/v) Pen-Strep solution (Gibco, USA), 2.5 mM L-glutamine (A5006, Sigma-Aldrich), 2.5 mM L-arginine (G8540, Sigma-Aldrich), sodium bicarbonate (2.2 g/L) and Hepes (2.6 g/L). hMSCs were cultured with α-MEM with GlutaMAX (Gibco) supplemented with 10% (v/v) FBS (ref. F7524, Sigma-Aldrich). hESCs were cultured with mTeSR™1 medium (ref. 85,850, STEMCELL Technologies). For this particular cell line, Matrigel® (ref 354,277, Corning hESC-qualified Matrix) was used to coat the T-flasks.

2.5. Cell-seeding in the microwell array insert for spheroid formation

Before use, each agarose microwell array produced was submerged in 3 mL of culture media in a 6-well plate overnight. Then, the culture medium from the inner part of the arrays was removed and 0.5 mL (array 1) or 1.5 mL (array 2) of hDPSCs suspension were dispensed in the microwell arrays while ensuring homogeneous distribution. The two types of microwell arrays were compared regarding their capacity to produce homogeneous spheroids through the analysis of cell aggregate morphology. Three cell seeding concentrations (0.5×10^6 1×10^6 and 2.5×10^6 cells per microwell array to hypothetically result in spheroids made of at least 3.048, 6.097 and 15.243 cells) and two different seeding approaches (static mode or moving in a spiral pattern, both performed manually) were tested. In the first seeding approach, both the pipette and the microwell array were kept in static mode and seeding was performed in a single point in the center of the structure. In the second approach, the pipette was moved following a spiral trajectory while dispensing constantly the cells in the microwell array. In all seeding experiments, cell concentration and viability were analyzed using the trypan blue (0.04%) exclusion method. Once the most appropriate combination between the number of cells per device and the approach to homogeneously seed the cells was defined, hMSCs and hESCs spheroids were produced.

To analyze the reproducibility of hMSC spheroids produced in large quantities with mold device 2, a total of ten independent devices were compared by evaluating the size and morphology of at least 17 spheroids randomly selected every 24 h, from day 1 to 5.

2.6. Monitoring of hMSCs spheroids aggregation and compaction processes

Time-lapse microscopy was performed for 54 h using a Nikon Eclipse TI-E microscope (Japan) with an Okolabs environmental control system (37 °C and 5% of CO_2 atmosphere) equipped with a Prime 95B sCMOS camera and Lumencor Spectra X Light source to study the formation process of the spheroids. First, the cells in the inoculum were stained at room temperature and in dark conditions for 30 min with the CellTracker™ deep red dye (15 μM in PBS, ref. C34565, Thermo Fischer) and with the Hoechst 33342 nucleic acid stain (15 μM in PBS, ref. H1399, Thermo Fischer) to facilitate the monitoring of cell movement and fusion. After this, the staining solution was removed, the cells were washed with PBS, resuspended in culture medium to reach 1×10^6 cells in 1.5 mL and seeded to form spheroids into the microwell array insert previously conditioned in 1.5 mL of culture medium. The remaining wells of the 6-well plate were filled with 1.5 mL of PBS each to avoid drying of the agarose mold during the time-lapse experiment. Immediately after cell seeding, 8 independent microwells chosen randomly were imaged every 30 min for 54 h using bright field, blue and red fluorescent filters to monitor cells marked with Hoechst 33342 staining and cell Tracker™, respectively.

2.7. Morphology characterization of spheroids produced for 7 days

To evaluate the performance of devices 1 and 2, spheroids of each tested cell densities (0.5×10^6, 1×10^6 and 2.5×10^6 cells per device) were analyzed after 48 h. All images were taken using an optical microscope with a 4× objective lens and analyzed regarding perimeter, circularity, sphericity and solidity using the Image J software functions (version 1.53e), while the diameters were determined manually using Image J.

To validate the versatility of device 2 to produce spheroids of three different cell types (hDPSCs, hMSCs, hESCs), spheroids initiated by the

Table 1
Qualitative parameters comparing different sterile molded microwell arrays obtained with ultrapure agarose (dissolved in NaCl 0.9%, PBS and supplemented culture medium), using different preparation conditions.

Conditions	Polymer and sterilization by autoclaving (121 °C, 15′, 1 bar)	Autoclaved ultrapure agarose powder				
	Concentration (% *w/v*)	2	3			
	Solution composition	0.9% NaCl		PBS	‹MEM with 10% FBS and 1% PEN/STREP	
	Preparation method	Dissolved by mixing and melting in microwave oven until about 90 °C			Dissolved by mixing and heating in a water bath at 56 °C	Dissolved by mixing and heating in a water bath at 37 °C
Results	Homogeneity of casted material	+ + +	+ + +	+ + +	+ + high volume of foam	+ not fully dissolved
	Easily unmolding without rupture	+ thin wall	+ + +	+ + +	+ + +	+ fragile
	Integrity of the microwell array (absence of fissures)	+ thin wall	+ + +	+ + +	+ + +	+ thin wall
	Quality of the cavities	+ + +	+ + +	+ + +	+ + +	+ + +
	Media leakage through the insert	+ +	not observed	not observed	not observed	+ +
	Stability during manipulation with tweezers after unmolding	+ + fragile	+ + +	+ + slippery	+ + +	+ + fragile
	Stability after 14 days in a cell incubator in the presence of culture medium (wet, 37 °C, 5% CO_2)	+ fragile	+ + +	+ + slippery	+ + +	+ fragile

inoculation of 1 × 10^6 cells per microwell array were analyzed on day 7. For that, an automated slide scanner microscope (Nikon Ti-E, Japan) was used before spheroid harvesting.

2.8. Spheroid viability analysis

The carboxyfluorescein succinimidyl ester (CFSE) dye (ref 21,888, Sigma-Aldrich) was used to analyze the viability of hDPSCs spheroids. Firstly, CFSE was solubilized at 5 mM in dimethylsulfoxide (DMSO) (ref. D2650, Sigma-Aldrich) and then diluted 100 times with Dulbecco's Phosphate-buffered Saline (DPBS) (ref. 14190144, Thermo Fisher). Sixty 7-day spheroids were washed twice with PBS and incubated in the CFSE/DPBS solution for 5 min in the dark at room temperature. Then, the spheroids were washed twice with DPBS, centrifuged (200*g*, 3 min), and observed in a Leica DM5500B fluorescence microscope coupled with a Leica DFC345 FX camera (Leica Microsystems CMS, GmbH, Germany).

A Live/Dead assay was performed to analyze the hMSCs viability. Briefly, sixty 7-day spheroids were washed twice with PBS, then incubated with a staining solution consisting of 2.5 μM of ethidium homodimer-1 (EthD-1, ref. E1169, Thermo Fisher) and 1 μM of calcein acetoxymethyl (Calcein AM, ref. c3099, Thermo Fisher) in PBS, for 30 min at 37 °C and 5% CO_2 atmosphere. After, the spheroids were washed with PBS and analyzed with a fluorescence microscope (Eclipse Ti-E Nikon, Japan) equipped with a monochromatic camera (Andor Zyla 5.5 sCMOS, Oxford Instruments, United Kingdom) and a Lumencor Spectra light source.

To monitor hESCs viability, the cells were previously transfected with a green fluorescent protein (GFP) gene, as described by de Castro et al. [44] Due to its constitutive and doxycycline-inducible expression, GFP fluorescence of transfected cells may have significant utility as a viability assay. Dark areas indicated loss of GFP fluorescence, demonstrating cell death. Firstly, doxycycline was added to the medium, in 80% confluent hESCs monolayer cell cultures, at a final concentration of 1 μg/mL, 48 h before detachment and preparation of the spheroids. Then, sixty 7-day spheroids were observed in a fluorescence microscope (DM5500B, Leica) coupled with a camera (DFC345 FX, Leica Microsystems CMS GmbH).

2.9. Immunocytochemistry and metabolic analysis of hDPSCs spheroids

Immunofluorescence analysis was performed to determine the growth of hDPSCs in spheroids through the use of a proliferating cell nuclear antigen. Sixty 7-day spheroids inoculated at a concentration of 1 × 10^6 cells per microwell array were incubated for 60 min in a 3% bovine serum albumin (BSA) solution in 0.1 M phosphate buffer at pH 7.4, followed by incubation with primary antibody for 4 h at room temperature. The anti-rabbit PCNA FL261 primary antibody (Santa Cruz, USA) was diluted (1/500) in a solution containing 1% BSA and 2% Triton X in 0.1 M phosphate buffer at pH 7.4. After 4 h, the specimens were rinsed with DPBS for 15 min and incubated with a donkey anti-rabbit Cy3-conjugated secondary antibody (Jackson Immunoresearch West Grove, PA, USA) diluted (1/250) in the same solution used to dissolve the primary antibody. After 45 min at room temperature under light protection, the spheroids were washed with DPBS and mounted with coverslips on aqueous glycerol solution (glycerin and distilled water, 3:1 *v*/v) containing 4,6′-diamidine-2-phenylindole dihydrochloride (DAPI, DNA dye, 1:1000, D9542, Sigma-Aldrich) and observed in a fluorescence microscope (DM5500B, Leica) coupled with a camera (DFC345 FX, Leica Microsystems CMS GmbH) utilizing rhodamine (CY3) and DAPI filters.

To analyze cellular metabolic activity, spheroids inoculated at a concentration of 1 × 10^6 cells per microwell array were cultured for up to 7 days. The culture medium was partially changed every 48 h by replacing one third of the spent medium with fresh solution. The spent culture medium aliquots were analyzed regarding pH and afterward, glucose and lactate quantifications were performed by enzymatic analysis in a multiparameter bioanalytical system (YSI 7100-06A, YSI, Yellow Springs, OH).

2.10. Statistical analysis

Statistical analysis was performed using GraphPad Prism Software (8.4.3 version). The Student's unpaired *t*-test was used to compare mean results from two independent samples, while for multiple comparisons, the Tukey's *post hoc* and ANOVA tests were employed (significance level considered for $p < 0.05$). All experiments were performed in at least three biological replicates. All data are expressed as mean ± standard deviation (SD) values or represented using standard deviation bars on the graphs.

3. Results

3.1. CAD design and mold device manufacture

The Polyjet technology was chosen based on the fact that complex freeform shapes can be printed in resin directly from a CAD model with high accuracy [45]. In this work, this technology showed to be appropriate to print the rigid device containing 164 micropillars, with excellent printing

fidelity (Fig. 2a-c) and satisfactory smooth finishes (Fig. 2d), even when considering the smaller features of the mold.

The method proved to be also sufficiently flexible to scale-up since the expansion of the spheroids manufacturing scale depends on the number of micropillars, which could be increased in two ways. The easiest way is to maintain a constant number of cavities and increase the number of devices to be used. Another strategy would require an adaptation of the CAD model to enlarge both the number of micropillars and the dimensions of the mold device, as a modular approach. In this case, for instance, a mold device with the dimensions of a Petri dish could be produced to obtain a massive number of spheroids, depending on the demand.

3.2. Manufacture of micromolded microwell array inserts

Mold device 1 was previously defined to obtain the microwell array inserts, and during this development step, a few drawbacks were identified and addressed. Mold device 2 is the result of all improvements done to obtain a higher volumetric capacity to perform more homogeneous cell seeding using diluted cell suspensions.

The optimization of the non-adhesive hydrogel composition using different concentrations of ultrapure agarose (dissolved in saline solution, PBS, or culture medium) was analyzed regarding qualitative parameters (as compiled in Table 1).

Using 2% agarose solution and mold device 1, thin walls and cracks were observed in the construct structure and consequently, culture medium leakage through the insert (Fig. 2e). Even though the use of mold device 2 partially improved the construct, only combining mold device 2 and agarose 3% solution turned possible to fully overcome these limitations, resulting in stable inserts easily manipulated after unmolding and sufficiently resistant to compression and manipulation using tweezers.

Compression tests were performed to analyze the necessary force to deform blocks specimens in 30% (Fig. 2f), to assess if the produced hydrogel inserts were sufficiently stable to be easily handled (Fig. 2g). When the microwell array insert was compressed and released by hand, it completely returned to its initial shape. Lower resistance was observed for gels produced with 2% agarose in 0.9% (*w/v*) NaCl solution and 3% agarose culture medium prepared at 37 °C, respectively, 10.1 ± 2.1 and 8.6 ± 2.1 N. The higher values were detected for 3% agarose solution in 0.9% (*w/v*) NaCl and 3% agarose culture medium prepared by heating to 56 °C, equal to 14.2 ± 2.2 and 14.5 ± 1.2 N, respectively.

By visual inspection, the block specimens made of 3% agarose culture medium prepared at 37 °C were considered homogeneous, but fragile. Heating only up to 37 °C was not enough to completely dissolve the agarose solution at 3%. Since the last two solutions presented statistically similar values, 3% agarose solution in 0.9% (w/v) NaCl heating up to 90 °C to ensure the complete dissolution of the agarose was chosen due to advantages related to cost and time required in hydrogel preparation. Thus, combining mold device 2 and 3% agarose solution in 0.9% (w/v) NaCl allowed obtaining mechanically stable, easily-handled micromolded microwell array inserts, with highly defined microstructure and no interconnection between wells.

We also investigated the stability of the agarose microwell array inserts during long periods in conditions used for cell culture (immersed in culture medium at 37 °C and 5% CO_2 atmosphere). The results are shown in Fig. 2h. By measuring the dimensions of the bottom part of the hexagons instantly after molding and after 2, 14 and 30 days in culture conditions, we observed that the microwell sides did not vary until day 14 (Fig. 2h). Changes in the microwell dimensions were observed at day 30, when retraction of the whole structure started to occur in all directions. One possible explanation is that the agarose hydrogel could have undergone mild sol-gel transition within 30 days at 37 °C [46], losing part of its mass over time. However, rearrangement of agarose chains could also have contributed to slightly shrink the overall dimensions while helping to maintain the general 3D structure of the microwell array inserts. Nonetheless, when immersed in culture medium at 37 °C and 5% CO_2 atmosphere, the tridimensional structure and the physical integrity of the microwell arrays were well-preserved for at least 14 days.

3.3. Morphology parameters of hDPSC spheroids obtained through mold devices 1 and 2

The performance of the microwell array inserts produced with mold devices 1 and 2 regarding spheroid morphology was compared for 7-day spheroids obtained with three different hDPSC seeding concentrations. Furthermore, the characteristics of spheroids produced at the border and in the center areas of the microwell array inserts (Fig. 3a) through two cell seeding approaches (static in a single point at the center or moving in a spiral pattern) were investigated.

For microwell array 1, the static cell seeding approach resulted in larger spheroids at the border (Fig. 3b, e) in contrast to spheroids produced in the center, with mean diameters of 288 ± 40 and 179 ± 22 μm, respectively. Even though the difference was reduced for the spiral cell seeding method (Fig. 3e), the spheroids produced at the border (270 ± 38 μm) had mean diameters statistically larger than those produced in the center (174 ± 19 μm). Varying cell numbers during seeding showed no particular effect or significant differences on final spheroid dimensions at day 7 (Fig. 3c-d).

In the case of microwell array 2, the spheroids from the border and center areas were statistically similar in size when produced using the spiral seeding approach for the three cell seeding densities (Fig. 3h). The change in the mold device design increased the microwell volume capacity, allowing for the use of a less concentrated cell suspension. This, in turn, resulted in a more uniform distribution of the cells in all microwells.

On day 7, the spheroids obtained showed mean diameters of 227 ± 16 μm (border) and 210 ± 18 μm (center) for 0.5×10^6 cells per insert, 285 ± 27 μm (border) and 283 ± 24 μm (center) for 1×10^6 cells per insert and 432 ± 33 μm (border) and 392 ± 41 μm (center) for 2.5×10^6 cells per insert. Thus, the microwells obtained using mold device 2 resulted in highly reproducible spheroids that were statistically similar in all regions of the microwell insert, differing only by the number of cells seeded (Fig. 3f-h). Spheroid size analysis performed along cell culture time indicated that the diameters could be precisely defined, resulting in significant differences between seeding densities and the final diameter at day 7 (Fig. 3i).

All cell spheroids produced by device molds 1 and 2 presented regular surfaces, showing solidity index higher than 0.96, and were considered spherical shaped structures, presenting sphericity index higher than 0.9 (both indexes considering a scale from 0 to 1).

The spheroids were analyzed regarding quality by visual inspection (Fig. 3j), considering the formation of protuberances, appendices, and satellite aggregates attached to the spheroid surface. Although the spiral seeding approach was observed to be slightly better than the static seeding during the performance analysis of microwell array 1, the presence of low-quality spheroids was more frequently detected in device 1 than in device 2. This was probably due to the high number of cells dispersed in a small amount of culture medium in device 1 during cell seeding. After these validation studies, all experiments were performed using microwell array 2 and cell seeding was done in spiral pattern.

To further investigate the applicability of the microwell array 2, three different cell types were produced with 1×10^6 cells per array, following the same procedures described above. Homogeneous spheroids were successfully produced in all cases, but cell type had a significant influence on the mean diameters of 7-day spheroids: 501 ± 25 μm for hESC; 253 ± 9 for hDPSCs and 221 ± 17 μm for hMSC. Regarding the sphericity index, all cell aggregates were considered spherical shaped structures (0.922 ± 0.01 μm for hESC; 0.913 ± 0.02 for hDPSCs and 0.916 ± 0.01 μm for hMSC, as observed in Fig. 3k).

3.4. Biological activity and morphological comparison between hDPSCs and hESCs spheroids

Cell viability of 7-day hDPSC and hESC spheroids was investigated. High cell viability was observed for hDPSC spheroids using the green

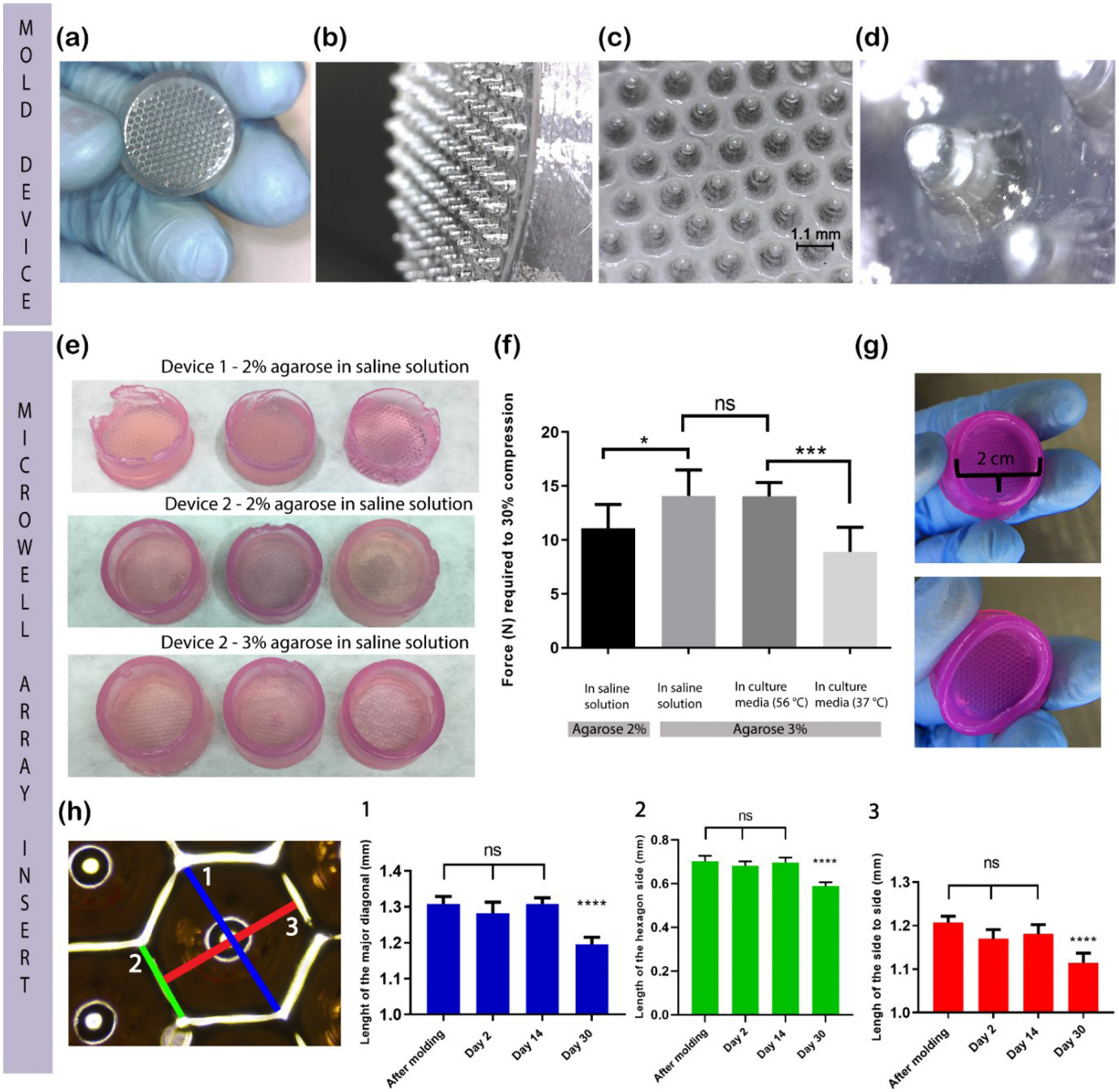

Fig. 2. a) General aspect of the mold device; b) lateral view of the mold device; c) detail on the smooth finish of the micropillars array; d) a printed micropillar in detail; e) structure of saline solution microwell arrays after incubation overnight in culture medium, varying the mold device and 2 and 3% agarose concentrations; f) results on non-confined compression testing of block specimens made of different agarose solutions, significant differences ***, $p < 0.001$, *, $p < 0.05$ and ns, non-significant differences for $p > 0.05$, as determined by the Tukey's multiple comparison test; g) When gently compressed by hand, the microwell array insert completely returned to its initial shape when released, showing adequate performance during manipulation; h) measurements of the major diagonal (blue), side (green) and side to side distance (red) of the hexagons immediately after demolding and at days 2, 14, and 30 in CO_2 cell incubator (10 hexagons of four independent devices were measured; ****, statistically significant differences $p < 0.001$, ns, non-significant).

fluorescent dye CFSE, which is capable of crossing the cell membrane and covalently binding to intracellular proteins (Fig. 4a). These cells show no visible signs of nuclei (DAPI, blue) fragmentation (Fig. 4g). Since the hESC cells were previously transfected with GFP, these cells were not stained with CFSE. The cells showed to be biologically active, profusely expressing GFP (Fig. 4b).

Interestingly, even when using the same seeding density (1×10^6 cells/insert), the mean diameter of hESC spheroids was around two times bigger than the average diameter of hDPSC spheroids at day 7 (Fig. 3k) (501 ± 25 μm and 253 ± 9 μm, respectively). This difference can be more clearly noticed in Fig. 4c. It was also possible to observe a difference in the distribution of cells in the whole 3D structure of these spheroids. Comparing Fig. 4a-b, a more tight and compact distribution of cells can be seen in hDPSC spheroids (Fig. 4a), in contrast with a more spread distribution of cells in the structure of hESC spheroids (Fig. 4b).

Taken together, these results show that aggregation of hDPSCs and hESCs cells differs and that the level of association and compaction of these two cell types to form spheroids might also vary. Finally, with the

clear influence of seeding density on spheroid dimension shown in Fig. 3, these results confirm that spheroid size is also strongly dependent on the type of cell used.

The volumetric capacity of the inner part of the optimized microwell array is 1.5 mL, which should be sufficient to be filled with culture medium to provide the main carbon and energy sources for the cells, as well as for maintaining cell homeostasis. To verify that, the metabolic activity of culturing 1×10^6 hDPSC cells per insert for six days regarding consumption of glucose (Fig. 4d) was monitored. Glucose uptake was considerable, reaching 57% in the first 48 h when the first medium refresh was performed. However, medium exchange would not be required before 48 h and the three sequential culture medium changes afterwards assured no glucose depletion. Since lactate is produced upon consumption of glucose, its synthesis was also monitored. Significant amounts of lactate were detected throughout the whole culture period (from 0.14 to 0.63 g/L). With its release, the pH was reduced from 7.32 to 6.5 after 144 h (Fig. 4e), and a control experiment performed with only culture medium, free of cells, showed practically no pH variation.

As discussed above, the viability of hDPSC on day 7 was high. Nevertheless, the amount of lactate detected in the microwell array at this time point was considerably high. To investigate if the cells were still reproducing at that point or started to become quiescent, a proliferating cell nuclear antigen (PCNA) assay was performed. As observed in Figs. 4f-h, hDPSC cells are still in proliferation after 7 days in culture, and despite being closely packed together, they show high PCNA expression.

3.5. Reproducibility analysis of the production of a large number of hMSC spheroids

To analyze the reproducibility of the procedures presented herein, a batch scaled to produce 1640 hMSCs spheroids was performed using 10 independent microwell arrays inoculated with 0.5×10^6 cells/microwell array (since 164 spheroids can be easily obtained with one array insert, a standard 6-well plate yields 984 spheroids, as shown in Fig. 5a).

Using an XY scanning microscope, it was possible to observe that at day 5, all spheroids were precisely kept in their specific seeding positions, even though culture medium exchange was performed three times and several handling movements were done with the plate (Fig. 5b). High cell viability could be detected in hMSCs spheroids using the Live/Dead assay (Fig. 5c), along with high metabolic activity assessed by the release of high levels of ATP (data not shown).

The hMSC spheroids obtained in the ten microwell arrays were analyzed in terms of diameter variation until day 5 (Fig. 5d). High spheroid size variation was determined immediately after cell seeding (0 h), but this variation was markedly reduced after 24 h. From 48 h on, the variations observed were not statistically significant. Since the CAD model was defined to offer a bottom circumference of 600 μm in diameter in the micromolded microwell arrays, the cells were able to randomly precipitate in this confined space, occupying initially approximately the whole area. The approximately round area occupied by the cells in all ten devices analyzed at 0 h had a diameter very close to that established in the CAD model, showing, therefore, that excellent shape fidelity could be achieved by using the designed microwell array, however, with some initial size variation. The mean diameter of the areas occupied by the cells immediately after seeding in all 10 microarrays was equal to 587 ± 28 μm, varying from averages around 539 to 630 μm, with minimum and maximum values equal to 467 to 686 μm, respectively.

According to the manufacturer [47], the accuracy range of the 3D printer used to produce the mold devices is within the range of 100 to 300 μm, and it can vary according to geometry, print size and structure orientation. These values, interestingly, were compatible with the variations observed for the initial mean diameters of the spheroids. At 24 h, the mean diameter was reduced to 278 ± 13 μm, and a much lower variation among the average and individual values for each device was noticed (*, $p < 0.05$). At the remaining times, no significant variation was observed in any case.

This is relevant evidence of the reproducibility of the method, as even though the diameter of the cavity may slightly vary during the device manufacturing, micromolding or demolding procedures (or even if the cells were deposited in different areas during seeding), the final diameter of the spheroids at day 5 is reproducible, with very low size distribution. Moreover, cell seeding had been done manually in this experiment, and this procedure can be easily automated with a robotic dispenser, potentially resulting in further reduction of size deviations.

3.6. Spheroid formation: aggregation and compaction phases

To elucidate how the aggregation of single cells took place and how fast this occurred, time-lapse microscopy was performed for 54 h using regular bright field microscopy (Supplementary Video 1), fluorescent staining with Hoechst 33342 cell nuclei blue stain (Supplementary Video 2), CellTracker™ deep red dye (Supplementary Video 3), and merged filters (Supplementary Video 4) to monitor the cells (representative images at selected time points shown in Fig. 5e and f). Although the staining ensured a better analysis of the fusion of cells into spheroids (thus avoiding visualization of agarose artifacts), the behavior of the individual cells was more clearly observed through phase-contrast bright field microscopy. The Hoechst 33342 blue staining was more effective for the visualization of individual cells, maintaining an intense fluorescence for long periods, while more diffuse images were obtained with the CellTracker™ red dye, which stains the cytoplasm.

The analysis of the morphological characteristics of the spheroids over time shows that two phases can be identified (Fig. 5d). In phase 1, from 0 h to 24 h, fast cell aggregation occurs, and loose cell aggregates start to be formed. Phase 2 takes place from 24 to 120 h, with this period characterized by the transition of aggregates from a looser and elongated structure (Fig. 5f, at the early hours of the monitoring period, phase 1 < 24 h) to a more stable and compact one (Fig. 5e, at the final hours of the study period, 120 h).

Spheroids harvested from the microwell array at 72 h (in the middle region of phase 2) and 120 h (final hour of phase 2) were compared (Fig. 5e). At 72 h, the hMSC spheroids produced were not completely formed, as can be noticed by the absence of a resistant outer region, which seemed to act as an envelope (red arrows, Fig. 5e). This envelope was present in spheroids harvested from the device at the end of phase 2. Additionally, at 72 h, it could be observed that the 3D structure of some spheroids dissembled in smaller aggregates (white arrows, Fig. 5e), and the presence of dispersed single cells is detected, mostly in the beginning. These facts were not observed at the end of phase 2 (120*h*), in which the 3D structure integrity of the spheroids was preserved.

4. Discussion

The purpose of this work was to optimize cost-competitive and customizable mold devices to create microwell array inserts with improved spheroid reproducibility from non-adhesive hydrogels. The rigid device molds created are reusable, and allow the production of a large number of hydrogel microwell arrays, which is very attractive in situations in which the reproducible generation of spheroids with uniform sizes is required in high throughput mode. As such, two different devices with different designs of increasing complexity were developed for this purpose.

First, a major modification was done to design the micropillars' geometry with a hybrid shape to optimize area usage and overcome some limitations observed with regular spherical form counterpart alternatives. Several reasons encouraged us to develop this complex hybrid shape, made of a bottom hexagon pyramidal structure and a top part defined by a semi-sphere. The regular spherical form commonly reported in the literature [48,49] tends to shrink due to water loss, compressing the forming spheroids. The bottom-hexagonal design avoids this problem, because six pillars support the geometric structure, and therefore, prevent the collapse to the center. This is relevant during spheroid formation and especially during the harvesting step since the spheroids should be easily released from the

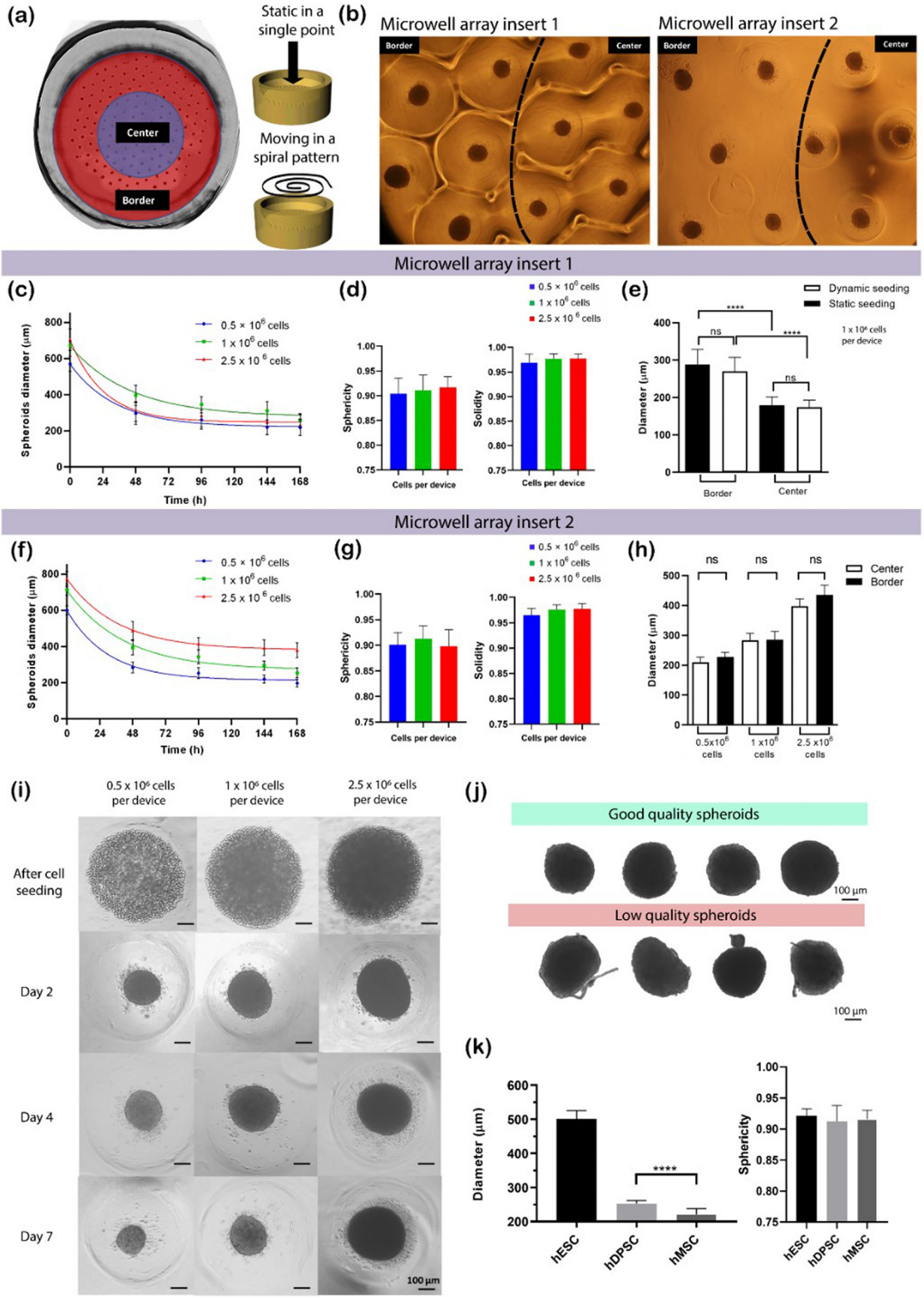

Fig. 3. Size and morphology of hDPSC spheroids obtained in microwell arrays 1 and 2: a) border and center areas of the microwell array insert and the two tested cell seeding approaches; b) spheroids differing in size produced in the border and center of microwell array 1; spheroids with similar size produced in the full area of microwell array 2, dashed lines represent the frontier between border and center areas; c) diameter variation during 7 day culture of spheroids in microwell array 1 (30 spheroids measured on each cell seeding); d) solidity and sphericity parameters of 7 day spheroids (30 spheroids measured on each cell seeding) produced with the microwell array 1; e) spheroids obtained at the border and center of microwell array 1 are statistically different with both cell seeding approaches (****, $p < 0.001$); f) diameter variation during 7 day culture of spheroids produced with microwell array 2 (30 spheroids measured on each cell seeding); g) solidity and sphericity parameters of 7 day spheroids (30 spheroids measured on each cell seeding) produced with microwell array 2; h) spheroids obtained at the border and center of microwell array 2 present no statistical differences with both cell seeding approaches (ns, not significant, $p > 0.05$); i) aggregation and compaction of hDPSC during 7 days to form spheroids with three different initial cell concentrations; j) quality analysis of hDPSCs spheroids; k) mean diameters and sphericity index of 7-day spheroids obtained with 10^6 cells per array of hESC, hDPSC and hMSC cells (20 spheroids measured of each cell type).

microwells, free of hydrogel residues. Additional handling and risk of contamination may happen when the spheroids are trapped inside the micromolded hydrogel. Using our device, spheroid harvesting can be easily performed by simply tilting the micromolded hydrogel at 90° and gently pipetting culture medium in the cavities, preventing cell exposure to excessive shear stress normally associated to the need of repetitive fluid displacement. Even though the top-hexagonal part offers space enough to do this, the bottom-hemisphere, in which the spheroids are produced, is closed enough to keep them in place during production. Refreshing of culture medium can also be easily performed in one step, without the risk of aspirating the spheroids, which is one of the most frequent complaints about the methods already available commercially. In addition, the bottom-hemisphere geometry was chosen over the regular cuspidal base of hexagonal structures to minimize negative effects on cell aggregate sphericity.

The regular spherical form also offers a dead space in between the circumferences in the multiarray micropillar. During cell seeding, a fraction of the cells could settle there and form tiny spheroids, instead of fully sedimenting into the microwell array cavities during the inoculation time. In a late stage, these detained cells grow and may be dragged into the cavities, attaching to the main cell aggregate in formation. As a result, satellite spheroids, bulges, and appendices anchor to the surface of the spheroid in formation, negatively affecting the spheroid quality. The hexagonal geometry allows, then, gentle dragging of the cells through the six edges to one or another cavity proximally located already during cell seeding. Stevens et al. [50] developed a multi-compartmental platform to produce different micropatterning from a PDMS substrate. Considering the pyramidal microwell designed to culture hepatocyte clusters, our findings corroborate with theirs, in which higher efficiency in cell capture is achieved due to the lack of dead spaces commonly noticed in spherical geometries. Thus, a significant increase in spheroid uniformity is observed, especially regarding surface characteristics, as well as precise control of cells seeded to result in useful spheroids.

The production of aggregates using similar non-commercial microwell arrays has been previously reported [51,52,53,54,55,56]. However, these systems were implemented through different manufacturing strategies, such as PDMS molding [53], CNC (computer numerical control) milling [51,54], microthermoforming [52] photolithography [55] and soft lithography [56]. The design of the micropillars' geometry also differ from our approach. Conventional cylindrical [51,52], spherical [53], conical [54], squared [55] and corner cubes [56] were often designed. The advantage of employing a high-resolution 3D Printer herein allowed the development of a novel complex hybrid shape, made of a bottom hexagon pyramidal structure and a top part defined by a semi-sphere. This improvement allowed overcoming limitations frequently observed for the conventional approaches, allowing the production of more uniform spheroids.

With our strategy, we aimed to obtain a reusable and cost-competitive microwell array, aiming to offer a positive effect on reproducibility and scale-up capability. Even though our approach involves the use of a sophisticated manufacturing technology, it is worth to emphasize that with the notable increase in demand and popularity and significant price reduction, 3D printers can be easily accessed from outsource printing services, or even leased for seasonal periods. Thus, purchasing a high-resolution printer is nowadays not mandatory. Considering these circumstances, and especially because the 3D printer will produce several reusable devices in one step, our approach is indeed a cost-effective alternative.

A few commercial alternatives are currently available for spheroid production based on microwell array systems. Some examples are the AggreWell™ system from Stemcell Technologies, MicroTissues® 3D Petri dish from Sigma-Aldrich and the 96-well Spheroid Ultra Low Attachment Microplates, by Corning. However, these systems are generally disposable or have limited usage, with the pre-manufactured design of the microcavities defined by the manufacturer. These are trivial drawbacks when commercial products are considered. On the other hand, these alternatives do not require sterilization, are ready-to-use and often are provided along with well-defined protocols and cell validation background. Through our approach, we focused on offering a reusable material as an alternative, as well as a low-cost system, since frequently a commercial product will be usually more expensive than a system developed in-house.

Thus, we focused on the optimization of the device design and the materials used to produce the hydrogel, as well as the process conditions that could strongly influence the quality and uniformity of the spheroids obtained. In this sense, a great improvement in the technology was demonstrated herein when comparing cell seeding and spheroid diameter obtained using devices 1 and 2. It was noticed that when a highly concentrated cell suspension was seeded, the cells tended to instantaneously sediment in a limited region of the device. The amount of culture medium used to disperse the high number of cells in device 1 (0.5 mL) is too low to allow homogeneous distribution of the cells throughout the whole device, reaching all the 164 cavities. Diluting the cell suspension three times significantly improved spheroid homogeneity because the larger amount of fluid phase available (1.5 mL in device 2) allowed the formation of a uniform liquid column 5.8 mm in height on top of the 164 microcavities, reducing the events of localized cell aggregation.

The validation of the device was performed through the cultivation of different categories of cells, with the main focus on human stem cells from different sources, two from adults (hDPSC and hMSC) and one from embryonic origin (hESC). The stem cells chosen show very particular properties, which allowed us to explore the effectiveness of the device to form spheroids with great integrity and quality, showing high uniformity and viability. hDPSC cells, for instance, have a high proliferation rate [57], which was confirmed in the immunostaining analysis, which showed that the cells were adapted enough to keep this growth pattern even when being cultured in aggregates for 7 days. hDPSC and bone marrow-derived MSC are known for producing large amounts of extracellular matrix [58], which contributes to cell-cell contact and improves the level of spheroid compaction in comparison to other stem cell types. On the other hand, hESC exhibit a higher growth rate *in vitro*, but less extracellular matrix production [44]. In fact, cell aggregation is driven not only by a spontaneous process of cell-cell interaction [59], but also by the way cells interact with ECM fibers, since the composition and concentration of ECM molecules may vary depending on the type of cell [60]. Corroborating this finding, our data demonstrated that after 7 days in culture, hESC spheroids were two times larger than hMSC spheroids. Besides, the mean diameter of 7-day old hESC spheroids (501 ± 25 μm) was very close to the microwell array diameter (600 μm) defined on the CAD model. It is worth mentioning that practically the same procedures were used to culture hMSC, hMSC and hESC to produce spheroids. The only variations were the culture media compositions, which were specific for each cell type, and the need to coat the T-flasks with Matrigel® to culture hESC cells. Thus, most probably the intercellular interactions of hMSC and hDPSC might be tighter and more intense than those observed for hESC cells.

The aggregation and compaction phases could barely be noticed in hESC spheroids. On the other hand, these phenomena were more intensively observed in two different stages for hMSC spheroids. The compaction phase 1 can be seen from 0 h to 24 h, in which primary aggregation of dispersed cells starts, and loose cell aggregates are formed. At this stage, cadherins, which play a key role in the intercellular interactions, are overexpressed [60], increasing cell cohesion and stiffness of the aggregates. Phase 2 takes place from 24 to 120 h, when it is possible to notice the transition of aggregates from a looser and elongated structure to a more rigid, stable, and compact structure [3]. The intercellular interactions of hMSC seem to be intense, as confirmed by the high diameter reduction observed (from a mean value of 587 ± 42 μm right after the cell seeding time to 222 ± 28 μm at day 7). As recently reviewed by Decarli et al. [29], initially, the cells contact each other and aggregate probably by the action of surface forces and cell migration. With time, intercellular interaction increases, and molecules associated to cell anchoring and adhesion, as well as extracellular matrix molecules, are produced in addition to cadherins (such as integrins, collagen I, and fibronectins), consolidating the spheroid, which shows a highly compact structure at the final hours of the study period.

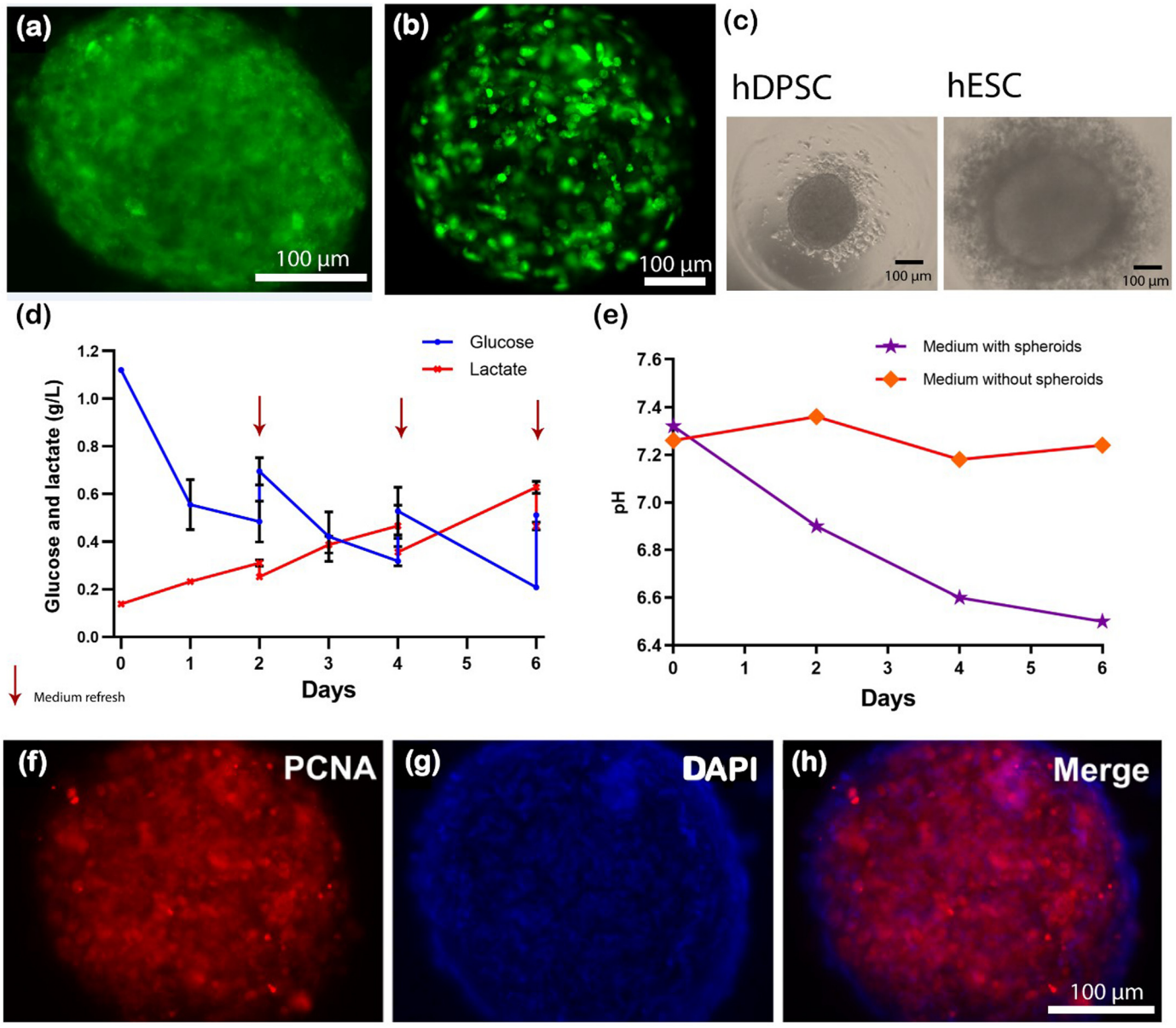

Fig. 4. Biological activity and morphological comparison of hDPSC and hESC 7-day spheroids produced with 1×10^6 cells/insert: a) staining of hDPSC in spheroids with CFSE (green); b) hESC in spheroids expressing GFP (green); c) aggregation and compaction analysis of hDPSC and hESC 7-day spheroids obtained with the same number of cells; d) metabolic profile of hDPSC single cells (0 h) during 7 days to form spheroids, based on the consumption of glucose and synthesis of lactate; e) pH of culture medium before medium exchange for hDPSC spheroids and a control group with the microwell array containing culture medium not inoculated with cells maintained in the incubator; f-h), proliferating cell nuclear marker (PCNA, red) and nuclei of cells (DAPI, blue) staining assay for hDPSC spheroids.

During the first 24 h, hMSC spheroid compaction, in terms of size reduction, reached 33% to 52%, depending on the presence or absence of the dyes (CellTracker™ deep red and Hoechst 33342 blue), respectively. After 48 h, compaction reached 45% and 57%, respectively, and after 54 h, spheroid dimensions were further reduced, but in a much lower proportion, to about 47% and 59% of their initial sizes. The kinetic behavior of hMSC cell aggregation and compaction may have been influenced by the presence of the dyes, mostly during phase 1. The dyes could have affected cell-cell and cell-matrix interactions, for instance, or reduced cell motility, slowing down mostly the initial aggregation steps.

As a whole, the spheroid production method presented herein offers relevant advantages, such as the potential to produce almost a thousand very uniform spheroids using only six micromolded arrays cast from a single reusable Veroclear™ device set in a conventional 6-well cell culture plate. Furthermore, the micromolded arrays are resistant and easily manipulated, allowing simple procedures for culture medium exchange and safe spheroid harvesting.

The usefulness of spheroids produced using the method presented herein was already tested in three preliminary studies. In the first one, it was observed that the microwell array can be successfully used to generate large amounts of spheroids at an affordable cost for bioprinting applications, as these cell aggregates gradually prove to be a more robust building block for large-size constructs than suspended isolated cells (data not shown). The second study showed that chondrogenic differentiation, a sensitive process, could be successfully performed on hMSC spheroids produced using the developed technology (Supplementary Fig. 2 shows the presence of GAG and collagen II, both main markers of chondrogenesis). Finally, in the third exploratory study, hESC spheroids were effectively used to access neuroprotective and immunomodulatory effects on spinal cord lesions (results not shown).

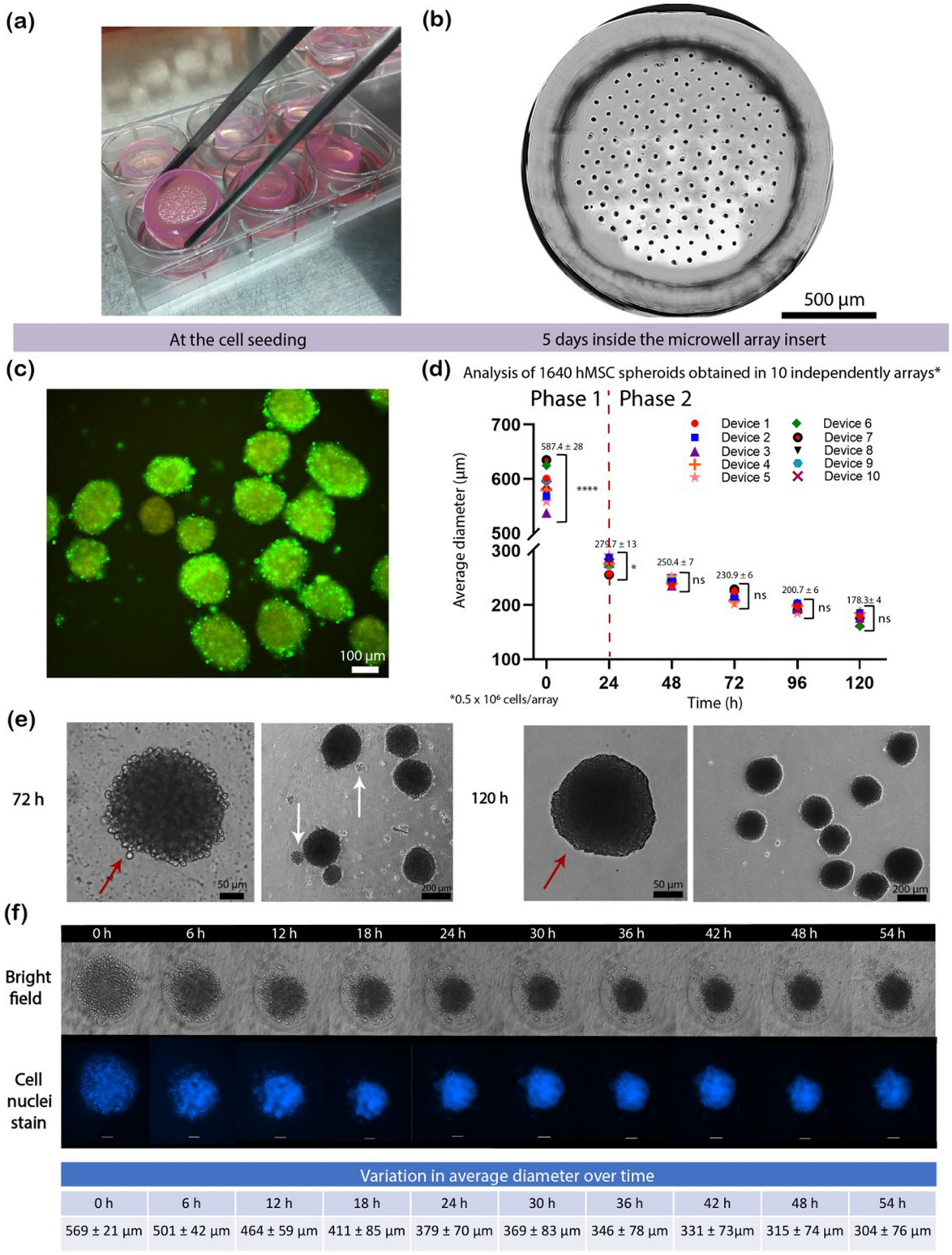

Variation in average diameter over time									
0 h	6 h	12 h	18 h	24 h	30 h	36 h	42 h	48 h	54 h
569 ± 21 µm	501 ± 42 µm	464 ± 59 µm	411 ± 85 µm	379 ± 70 µm	369 ± 83 µm	346 ± 78 µm	331 ± 73µm	315 ± 74 µm	304 ± 76 µm

Fig. 5. Aggregation and compaction phases of hMSC spheroids in the micromolded arrays: a) setting of six arrays in a 6-well plate to produce a total of 984 spheroids per plate; b) XY scanning microscopy showing 164 spheroids precisely kept in the cavities of one micromolded array at day 5; c) staining of live cells of hMSC 5-day old spheroids (calcein, Live/Dead assay, green); d) size variation of hMSC spheroids in 10 independent microwell arrays (each of the ten symbols in the graph represents the mean diameter ± SD of 17 spheroids of that array measured at the specified time). The values provided were calculated considering variation within individual arrays and between arrays, using Tukey's multiple comparison test (95% CI), with 45 combinations tested per time point to analyze significant differences at each time in comparison to initial cell aggregate size immediately after seeding (****, $p < 0.001$) and after 24 h (*, $p < 0.05$). From 48 to 120 h, the differences in each group are not statistically significant (ns); e) morphological comparison between spheroids during the transition period in phase 2. At 72 h, spheroids were not completely formed (red arrow) and some of them disassembled in smaller aggregates when removed from the microwell insert (white arrows). At 120 h, rigid, compact spheroids were observed, with a resistant outer region enveloping the cell aggregate (red arrow); f) Representative images of time-lapse microscopy analysis performed for 54 h (scale bars equal to 100 µm). Time-lapse videos are available in Supplementary Videos 1-4.

Overall, the method presented here showed high effectiveness and reproducibility, which are mandatory to guarantee efficacy and safety requirements during pre-clinical studies and other uses for cell spheroids. Moreover, the method demonstrated is robust, can be implemented in a low-cost approach, and offers an alternative to minimize animal usage.

5. Conclusion

By casting a microwell array insert using a non-adhesive hydrogel to obtain a device with highly regular microcavities we provided a simple, feasible and affordable method to produce 3D models of human microtissues in the form of homogeneous spheroids that can be easily implemented in laboratory routine. The results have shown that 3D culturing of hDPSC, hMSC and hESC yielded a large number of uniform and viable spheroids, useful for many research and clinical purposes.

Supplementary data to this article can be found online at https://doi.org/10.1016/j.msec.2022.112685.

CRediT authorship contribution statement

Monize Caiado Decarli: Conceptualization, methodology, software, validation, formal analysis, investigation, data curation, writing - original draft, writing - review & editing, visualization.

Mateus Vidigal de Castro: Methodology, validation, formal analysis, investigation, visualization.

Júlia Adami Nogueira: Methodology, investigation, visualization.

Mariana Harue T. Nagahara: Methodology, investigation, visualization.

Cecília Buzatto Westin: Methodology, investigation, visualization.

Alexandre Leite R. de Oliveira: Methodology, validation, formal analysis, resources, writing - review & editing, visualization.

Jorge Vicente L. Silva: Conceptualization, software, validation, formal analysis, resources, data curation, writing - review & editing, visualization, supervision, project administration, funding acquisition.

Lorenzo Moroni: Conceptualization, methodology, validation, formal analysis, resources, data curation, writing - review & editing, visualization, supervision, project administration, funding acquisition.

Carlos Mota: Conceptualization, software, methodology, formal analysis, resources, data curation, writing - review & editing, visualization, supervision, project administration, funding acquisition.

Ângela Maria Moraes: Conceptualization, methodology, validation, formal analysis, resources, data curation, writing - review & editing, visualization, supervision, project administration, funding acquisition.

Declaration of competing interest

The authors Monize Caiado Decarli, Júlia Adami Nogueira, Jorge Vicente L. Silva and Ângela Maria Moraes declare that they have applied for a patent application for the mold device and its use at the Brazilian National Institute of Industrial Property, under the registration number BR 102019 0273607, in Brazil, in December 2019.

Acknowledgments

The authors would like to acknowledge the support to this research by: the National Council for Scientific and Technological Development (Conselho Nacional de Desenvolvimento Científico e Tecnológico – CNPq, Brazil – Grants # 307829/2018-9, 430860/2018-8 and 142050/2018-0); the Coordination for the Improvement of Higher Educational Personnel (Coordenação de Aperfeiçoamento de Pessoal de Nível Superior CAPES, Brazil - Finance codes 001, PrInt 88887.364849/2019-00 and PrInt 88887.310405/2018-00); the Fund for Support to Teaching, Research and Extension from the University of Campinas (Fundo de Apoio ao Ensino, à Pesquisa e à Extensão - FAEPEX/UNICAMP, Brazil - Grants # 2921/18, 2324/21); the São Paulo Research Foundation (Fundação de Amparo à Pesquisa do Estado de São Paulo - FAPESP, Brazil, INCT-REGENERA, Grant # 465656/2014-5) and the European Union's Horizon 2020 framework program, call SC1-BHC-07-2019, under grant agreement 874837.

The authors would also like to thank MSc. Adrián Seijas Gamardo and Dr. Paul Wieringa (Maastricht University, The Netherlands) for the support on the time-lapse microscopies and Dr. Robson Luis Ferraz do Amaral and Prof. Dr. Kamilla Swiech (University of São Paulo, Brazil) for the metabolic analysis performed on hDPSC spheroids.

References

[1] D. Loessner, K.S. Stok, M.P. Lutolf, D.W. Hutmacher, J.A. Clements, S.C. Rizzi, Biomaterials 31 (2010) 8494.
[2] S. Sant, P. Johnston, Drug Discov. Today Technol. 23 (2017) 27.
[3] S. Sart, A.-C. Tsai, Y. Li, T. Ma, Tissue Eng. Part B 20 (2014) 365.
[4] R.L.F. Amaral, M. Miranda, P.D. Marcato, K. Swiech, Front. Physiol. 8 (2017) 1.
[5] C. Wenzel, B. Riefke, S. Gründemann, A. Krebs, S. Christian, F. Prinz, M. Osterland, S. Golfier, S. Räse, N. Ansari, M. Esner, M. Bickle, F. Pampaloni, C. Mattheyer, E.H. Stelzer, K. Parczyk, S. Prechtl, P. Steigemann, Exp. Cell Res. 323 (2014) 131.
[6] M.C. Pearce, J.T. Gamble, P.R. Kopparapu, E.F. O'Donnell, M.J. Mueller, H.S. Jang, J.A. Greenwood, A.C. Satterthwait, R.L. Tanguay, X.-K. Zhang, S.K. Kolluri, Oncotarget 9 (2018) 26072.
[7] M.A. Theodoraki, C.O. Rezende, O. Chantarasriwong, A.D. Corben, E.A. Theodorakis, M.L. Alpaugh, Oncotarget 6 (2015) 21255.
[8] S.D. Ramachandran, K. Schirmer, B. Münst, S. Heinz, S. Ghafoory, S. Wölfl, K. Simon-Keller, A. Marx, C.I. Oie, M.P. Ebert, H. Walles, J. Braspenning, K. Breitkopf-Heinlein, PLoS One 10 (2015) 1.
[9] C.C. Bell, A.C.A. Dankers, V.M. Lauschke, R. Sison-Young, R. Jenkins, C. Rowe, C.E. Goldring, K. Park, S.L. Regan, T. Walker, C. Schofield, A. Baze, A.J. Foster, D.P. Williams, A.W.M. van de Ven, F. Jacobs, J. van Houdt, T. Lähteenmäki, J. Snoeys, S. Juhila, L. Richert, M. Ingelman-Sundberg, Toxicol. Sci. 162 (2018) 655.
[10] S.D. Forsythe, M. Devarasetty, T. Shupe, C. Bishop, A. Atala, S. Soker, A. Skardal, Front. Public Heal. (2018) 6.
[11] M. Takasato, P.X. Er, H.S. Chiu, B. Maier, G.J. Baillie, C. Ferguson, R.G. Parton, E.J. Wolvetang, M.S. Roost, S.M.C. Lopes, M.H. Little, Nature 526 (2015) 564.
[12] D. Simão, F. Arez, A.P. Terasso, C. Pinto, M.F. Sousa, C. Brito, P.M. Alves, Methods Mol. Biol. 1502 (2016) 129.
[13] M. Huch, J.A. Knoblich, M.P. Lutolf, A. Martinez-Arias, Development 144 (2017) 938.
[14] M.P. Stuart, R.A.M. Matsui, M.F.S. Santos, I. Côrtes, M.S. Azevedo, K.R. Silva, A. Beatrici, P.E.C. Leite, P. Falagan-Lotsch, J.M. Granjeiro, V. Mironov, L.S. Baptista, Stem Cells Int. (2017) 1.
[15] K. Murphy, S. Fang, K. Leach, Cell Tissue Res. 357 (2014) 91.
[16] A.C. Daly, D.J. Kelly, Biomaterials 197 (2019) 194.
[17] V. Mironov, R.P. Visconti, V. Kasyanov, G. Forgacs, C.J. Drake, R.R. Markwald, Biomaterials 30 (2009) 2164.
[18] C. Mota, S. Camarero-Espinosa, M.B. Baker, P. Wieringa, L. Moroni, Chem. Rev. 120 (2020) 10547.
[19] C.M. Owens, F. Marga, G. Forgacs, C.M. Heesch, Biofabrication 5 (2013), 045007.
[20] R.P. Visconti, V. Kasyanov, C. Gentile, J. Zhang, R.R. Markwald, V. Mironov, Expert. Opin. Biol. Ther. 10 (2010) 409.
[21] T. Boland, V. Mironov, A. Gutowska, E.A. Roth, R.R. Markwald, Anat. Rec. Part A 272 (2003) 497.
[22] E. Vrij, S. Espinoza, M. Heilig, A. Kolew, M. Schneider, C.A. Van Blitterswijk, R.K. Truckenmüller, N.C. Rivron, Lab Chip 16 (2016) 734.
[23] I. Fraietta, F. Gasparri, Expert Opin. Drug Discov. 11 (2016) 501.
[24] P. Joshi, A. Datar, K.N. Yu, S.Y. Kang, M.Y. Lee, Toxicol. Vitr. 50 (2018) 147.
[25] G.A. Higuera, J.A.A. Hendriks, J. Van Dalum, L. Wu, R. Schotel, L. Moreira-Teixeira, M. Van Den Doel, J.C.H. Leijten, J. Riesle, M. Karperien, C.A. Van Blitterswijk, L. Moroni, Integr. Biol. 5 (2013) 889.
[26] K. Ronaldson-Bouchard, G. Vunjak-Novakovic, Cell Stem Cell 22 (2018) 310.
[27] B.W. Huang, J.Q. Gao, J. Control. Release 270 (2018) 246.
[28] A. Amelian, K. Wasilewska, D. Megias, K. Winnicka, Pharmacol. Rep. 69 (2017) 861.
[29] M.C. Decarli, R.L.F. Amaral, D.P. dos Santos, L.B. Tofani, E. Katayama, R.A. Rezende, J.V.L. Silva, K. Swiech, C.A.T. Suazo, C. Mota, L. Moroni, A.M. Moraes, Biofabrication 13 (2021) 032002.
[30] S. Sart, T. Ma, Y. Li, Biotechnol. Prog. 29 (2013) 143.
[31] M. Zanoni, F. Piccinini, C. Arienti, A. Zamagni, S. Santi, R. Polico, A. Bevilacqua, A. Tesei, Sci. Rep. 6 (2016) 1.
[32] L. De Moor, I. Merovci, S. Baetens, J. Verstraeten, P. Kowalska, D.V. Krysko, W.H. De Vos, H. Declercq, Biofabrication 10 (2018), 035009.
[33] J.P. Freyer, R.M. Sutherland, Cancer Res. 46 (1986) 3504.
[34] K. Groebe, W. Mueller-Klieser, Int. J. Radiat. Oncol. 34 (1996) 395.
[35] R.A. Foty, M.S. Steinberg, Wiley Interdiscip. RevDev. Biol. 2 (2013) 631.
[36] M. Yu, A. Mahtabfar, P. Beelen, Y. Demiryurek, D. Shreiber, J. Zahn, R. Foty, L. Liu, H. Lin, Biophys. J. 114 (2018) 2703.
[37] Achilli, J. Meyer, J. Morgan, Expert Opin. Biol. Ther. 12 (2012) 1347.
[38] K. Moshksayan, N. Kashaninejad, M.E. Warkiani, J.G. Lock, H. Moghadas, B. Firoozabadi, M.S. Saidi, N.T. Nguyen, Sensors ActuatorsB Chem. 263 (2018) 151.
[39] M. Rogers, T. Sobolik, D.K. Schaffer, P.C. Samson, A.C. Johnson, P. Owens, S.G. Codreanu, S.D. Sherrod, J.A. McLean, J.P. Wikswo, A. Richmond, Biomicrofluidics 12 (2018) 1.
[40] V.E. Santo, M.F. Estrada, S.P. Rebelo, S. Abreu, I. Silva, C. Pinto, S.C. Veloso, A.T. Serra, E. Boghaert, P.M. Alves, C. Brito, J. Biotechnol. 221 (2016) 118.
[41] M. Barisam, M. Saidi, N. Kashaninejad, N.-T. Nguyen, Micromachines 9 (2018) 94.

[42] M.C. Decarli, A.M. Moraes, J.V.L.Da Silva, J.A. Nogueira, J.A. Dernowsek, P.Inforçatti Neto, R.A. Rezende, F.D.A.S. Pereira, V. Mironov, Micromold for the Production of Cell Spheroids and Use. Patent Deposit from the Brazilian National Institute of Industrial Property - BR 10 2019 0273607, 2019 BR 10 2019 0273607.
[43] L. Wu, J.C.H. Leijten, N. Georgi, J.N. Post, C.A. Van Blitterswijk, M. Karperien, Tissue Eng. Part A 17 (2011) 1425.
[44] M.V. de Castro, M.V.R. da Silva, G.B. Chiarotto, M.H. Andrade Santana, Â.C. Malheiros Luzo, S. Kyrylenko, A.L.R. de Oliveira, Stem Cells Int. 2020 (2020) 1.
[45] C.B.L. Ulbrich, C.A.C. Zavaglia, P.Inforçatti Neto, M.F. Oliveira, J.V.L. Silva, 5th Int. Conf. Adv. Res. Virtual Phys. Prototyping, VR@P 2011, 573, 2012.
[46] C.D. Mahesh, R.V. Bellamkonda, in: R.M.N. Anthony Atala, Robert Lanza, James A. Thomson (Eds.), Princ. Regen. Med, Academic Press 2008, pp. 1270–1285.
[47] Objet, Multi-material 3-Dimensional Printing System - Connex 350, 2009.
[48] A.P. Napolitano, D.M. Dean, A.J. Man, J. Youssef, D.N. Ho, A.P. Rago, M.P. Lech, J.R. Morgan, Biotechniques 43 (2007) 494.
[49] A.P. Napolitano, P. Chai, D.M. Dean, J.R. Morgan, Tissue Eng. 13 (2007) 2087.
[50] K.R. Stevens, M.D. Ungrin, R.E. Schwartz, S. Ng, B. Carvalho, K.S. Christine, R.R. Chaturvedi, C.Y. Li, P.W. Zandstra, C.S. Chen, S.N. Bhatia, Nat. Commun. 4 (2013) 1.
[51] S. Lee, S. Kim, J. Ahn, J. Park, B.Y. Ryu, J.Y. Park, Biofabrication 12 (2020) 1.
[52] P. Kakni, R. Hueber, K. Knoops, C. López-Iglesias, R. Truckenmüller, P. Habibovic, S. Giselbrecht, Adv. Biosyst. 4 (2020) 1.
[53] L. de Moor, I. Merovci, S. Baetens, J. Verstraeten, P. Kowalska, D.V. Krysko, W.H. de Vos, H. Declercq, Biofabrication 10 (2018), 035009.
[54] A.R. Thomsen, C. Aldrian, P. Bronsert, Y. Thomann, N. Nanko, N. Melin, G. Rücker, M. Follo, A.L. Grosu, G. Niedermann, P.G. Layer, A. Heselich, P.G. Lund, Lab Chip 18 (2018) 179.
[55] H.S. Shin, H.J. Hong, W.G. Koh, J.Y. Lim, ACS Biomater. Sci. Eng. 4 (2018) 4311.
[56] J. Dahlmann, G. Kensah, H. Kempf, D. Skvorc, Anke Gawol, D.A. Elliott, G. Dräger, R. Zweigerdt, U. Martin, Ina Gruh, Biomaterials 34 (2013) 2463.
[57] B. Li, Y. Jin, Stem Cell Biol. Tissue Eng. Dent. Sci, Academic Press 2015, p. 471.
[58] A. Mizukami, C.H. Thomé, G.A. Ferreira, G.P. Lanfredi, D.T. Covas, S.J. Pitteri, K. Swiech, V.M. Faça, Front. BioengBiotechnol. 7 (2019) 1.
[59] S. Crawford, D. Diamond, L. Brustolon, R. Penarreta, Cancer Microenviron. 4 (2011) 93.
[60] I. Smyrek, E. Mathew, S.C. Fisher, S.M. Lissek, S. Becker, E.H.K. Stelzer, Biol. Open 8 (2019) bio037051.